JCTC Journal of Chemical Theory and Computation

Article

pubs.acs.org/JCTC

Potential Application of Alchemical Free Energy Simulations to Discriminate GPCR Ligand Efficacy

Hui Sun Lee,[†] Chaok Seok,[‡] and Wonpil Im*[,†]

[†]Department of Molecular Biosciences and Center for Computational Biology, The University of Kansas, 2030 Becker Drive, Lawrence, Kansas 66047, United States

[‡]Department of Chemistry, Seoul National University, Seoul 151-747, Republic of Korea

Supporting Information

ABSTRACT: G protein-coupled receptors (GPCRs) play fundamental roles in physiological processes by modulating diverse signaling pathways and thus have been one of the most important drug targets. Based on the fact that GPCR-mediated signaling is modulated in a ligand-specific manner such as agonist, inverse agonist, and neutral antagonist (termed ligand efficacy), quantitative characterization of the ligand efficacy is essential for rational design of selective modulators for GPCR targets. As experimental approaches for this purpose are time-, cost-, and labor-intensive, computational tools that can systematically predict GPCR ligand efficacy can have a big impact on GPCR drug design. Here, we have performed free energy perturbation molecular dynamics simulations to calculate absolute binding free energy of an inverse agonist, a neutral antagonist, and an agonist to β_2-adrenergic receptor (β_2-AR) active and inactive states, respectively, in explicit lipid bilayers. Relatively short alchemical free energy calculations reveal that both the time-series of the total binding free energy and decomposed energy contributions can be used as relevant physical properties to discriminate β_2-AR ligand efficacy. This study illustrates a merit of the current approach over simple, fast docking calculations or highly expensive millisecond-time scale simulations.

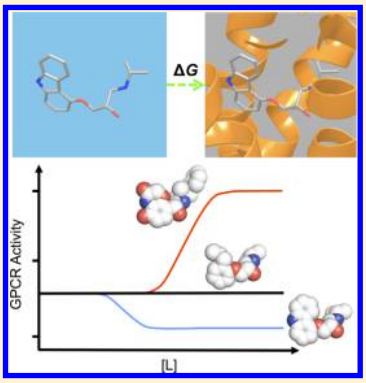

INTRODUCTION

G protein-coupled receptors (GPCRs) constitute the largest protein superfamily in the human genome with almost 1,000 members. They play key functional roles as major contributors of information flow from the outside to the inside of the cell, making them one of the most important protein families. As a result of their broad influence on human physiology and behavior, GPCRs are arguably the most promising targets for development of new and more effective therapeutic agents.[1] Indeed, it has been estimated that more than a half of all available drugs and more than a quarter of new drugs target GPCRs directly or indirectly.[2−4]

The action of ligands on receptors can be described by two events: affinity and efficacy. Affinity is the ability of ligands to bind to the receptor, while efficacy represents their effects on the receptor signaling. GPCR-mediated signaling is also modulated by ligands with varying efficacy.[5] GPCR ligands can be mostly classified into inverse agonist, neutral antagonist, and agonist depending on their efficacy, as illustrated schematically in Figure 1A. The basal level of GPCR activity, exhibited even in the absence of agonist,[6] can be suppressed by inverse agonists or further activated by agonists. A receptor can be maximally activated by full agonists or partially activated by partial agonists. Neutral antagonists block binding of other ligands without altering the basal activity. Some biased agonists/antagonists can also affect the same signaling through G protein-independent pathways.[7,8]

β_2-adrenergic receptor (β_2-AR), an important target for airway and cardiovascular diseases, is a well-studied GPCR system used to elucidate the underlying molecular mechanism of GPCRs. Importantly, β_2-AR is one of the few GPCRs whose high-resolution crystal structures of both inactive and active conformations in complex with diffusible ligands are available.[9−13] Comparison between the active and inactive β_2-AR conformations shows that relatively subtle changes in the ligand binding pocket lead to large conformational changes near the G protein-binding cytoplasmic surface (Figure 2A,C).[12]

In addition to this unprecedented static structural information, there are also ample experimental data about dynamic features of GPCRs. First, an NMR study using $^{13}CH_3\varepsilon$-Mets showed that agonist binding does not fully stabilize the active conformation of β_2-AR but destabilizes the inactive state. This study also suggested conformational heterogeneity in agonist-bound β_2-AR, implying multiple signaling networks and regulatory proteins engaged in β_2-AR-mediated signaling.[14] Second, a ^{19}F NMR study revealed two distinct inactive states and an activation intermediate of β_2-AR. In particular, analysis of the spectra as a function of temperature showed remarkably low β_2-AR enthalpy changes and positive entropy changes toward activation, indicating great mobility in the cytoplasmic domain.[15] Third, the crystal structure of β_2-AR

Received: October 6, 2014
Published: February 11, 2015

DOI: 10.1021/ct5008907
J. Chem. Theory Comput. 2015, 11, 1255−1266

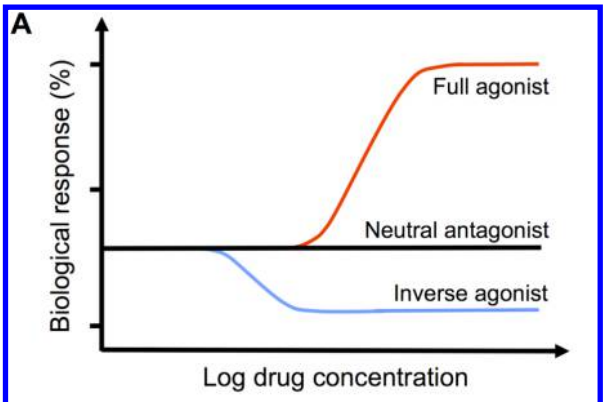

B

Ligand	Efficacy	Exp. K	Exp. ΔG_b (kcal/mol)
Carazolol	Inverse agonist	0.114 nM (K_i)	-13.65
Alprenolol	Neutral antagonist	0.910 nM (K_D)	-12.41
BI-167107	Full agonist	0.084 nM (K_d)	-13.83

Figure 1. Experimental efficacy of β_2-adrenergic receptor (β_2-AR) ligands and their binding affinities.

with covalently bound agonist (without G protein) did not show the global conformational changes expected for the active state (with respect to the inactive conformation), although the complex activated G protein in vitro. This finding indicates higher stability of the inactive conformation than the active conformation as well as the need of G protein to stabilize the active conformation.[16] Finally, a growing body of evidence suggests that GPCRs have an ensemble of conformations (each with a distinct population), and activation of GPCRs occurs through a series of conformational intermediates upon ligand binding. The fact that structurally diverse β_2-AR ligands have relatively low affinity and rapid dissociation rates also suggests ligand binding by conformational selection.[17]

Such high structural plasticity of GPCRs makes the development of selective GPCR drugs a daunting task. In general, potential drug candidates are screened in terms of their affinity to target proteins because higher affinity usually ensures better activity. For proteins like GPCRs, however, ligand efficacy and affinity do not show a simple relationship[10] because they are an outcome of sophisticated and delicate interplay of ligand with dynamic structures (i.e., functional states) of GPCRs. For example, as shown in Figures 1B and 2B, three ligands of β_2-AR, carazolol, alprenolol, and BI-167107, do not have largely different binding affinity but show distinct efficacy as an inverse agonist, a neutral antagonist, and a full agonist, respectively.

Since the report of Weiland et al. on a fundamental difference between the molecular interactions of antagonists and agonists with the β-adrenergic receptor,[18] there have been significant endeavors to measure biophysical properties of various GPCR ligands to discriminate their efficacy.[19−22] However, molecular-level biophysical characterization of GPCR ligands' efficacy falls

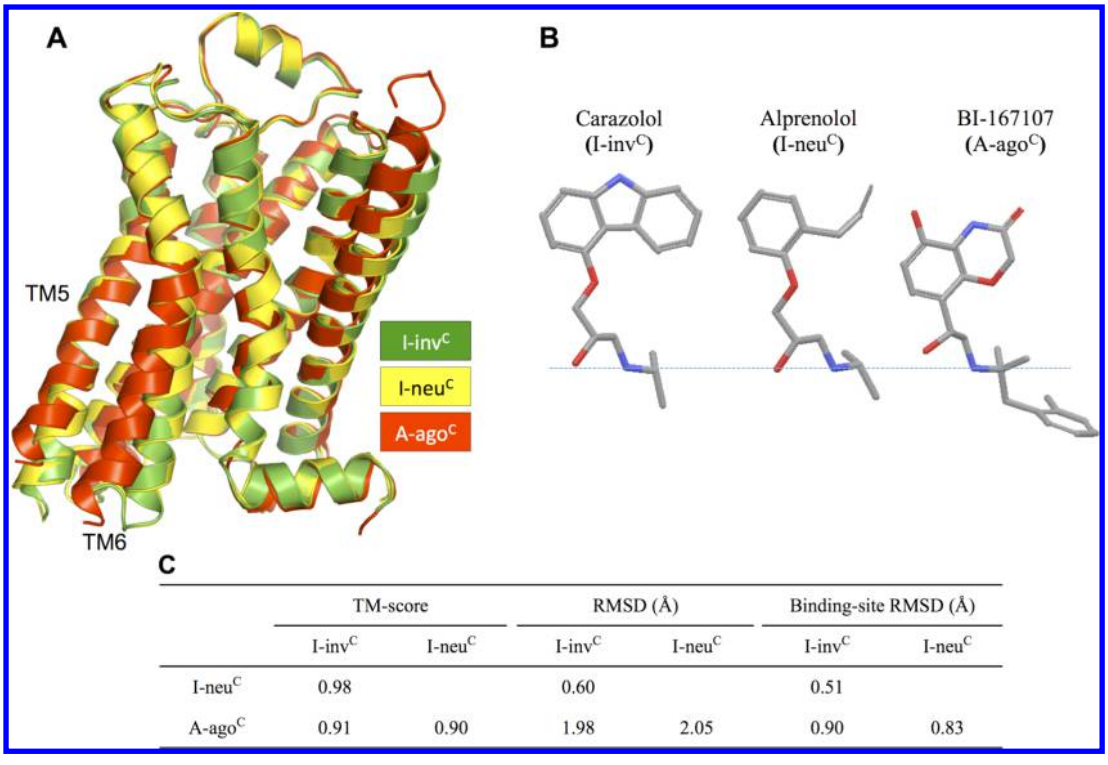

C

	TM-score		RMSD (Å)		Binding-site RMSD (Å)	
	I-inv^C	I-neu^C	I-inv^C	I-neu^C	I-inv^C	I-neu^C
I-neu^C	0.98		0.60		0.51	
A-ago^C	0.91	0.90	1.98	2.05	0.90	0.83

Figure 2. Comparison of β_2-AR crystal structures with inverse agonist, neutral antagonist, and full agonist. (A) The structures of inverse agonist carazolol-bound, neutral antagonist alprenolol-bound, and full agonist BI-167107-bound β_2-AR are shown in green, yellow, and red, respectively. (B) Structural comparison of carazolol, alprenolol, and BI-167107. A dotted (blue) line indicates the positively charged nitrogen of the ligands that interacts with Asp$^{3.32}$ conserved in aminergic receptors. The protein structures were superposed by TM-align[63] using Cα atoms. PyMol (http://www.pymol.org) and Maestro (Schrödinger, LLC) were used for the preparation of the figures. (C) Global structure TM-scores and RMSDs as well as binding-site RMSDs between different crystal structures of β_2-AR. The binding-site residues were defined by a distance cut of 4.5 Å between receptor and ligand heavy atoms in inverse agonist-bound inactive β_2-AR.

DOI: 10.1021/ct5008907
J. Chem. Theory Comput. 2015, 11, 1255−1266

far short of large-scale approaches due to the experimental difficulties of handling dynamic integral membrane proteins.

With the recent innovative development in GPCR crystallography, structure coverage of GPCRs has been greatly expanded, offering a prospect that the high-resolution structures of diverse intermediate states for representative GPCRs from a majority of subfamilies will be available within the next decade.[23] These structures will be able to provide much opportunity for structure-based computational drug design. Furthermore, the computational models predicted from additional structure templates are anticipated to provide more reliable theoretical data.

Molecular docking is a fast computational method to obtain binding modes and binding affinity of a compound to a target protein. However, the binding affinity predicted by this method is not only inaccurate in general[24] but also does not provide any information on ligand efficacy mainly due to its inability to take into account the fully dynamic nature of proteins upon docking. On the other hand, atomistic molecular dynamics simulations on a millisecond time scale can provide insight into GPCR ligand efficacy by characterizing how the ligands modulate the receptor dynamics.[25] However, this approach is computationally too expensive and not currently available to most researchers.

In this study, we perform free energy perturbation molecular dynamics (FEP/MD) simulations in explicit lipid bilayers to calculate absolute binding free energies to explore the molecular basis of β_2-AR ligand efficacy. Carazolol, alprenolol, and BI-167107 are considered as the representative inverse agonist, neutral antagonist, and full agonist of β_2-AR, and each ligand is complexed with both active and inactive β_2-AR states, yielding a total of six FEP/MD simulation systems. Relatively short FEP/MD simulations reveal that both the time-series of the total binding free energy and decomposed energy contributions can be used as relevant physical properties to discriminate the efficacy of GPCR ligands along with other valuable insights into ligand specificity and action mechanisms.

MATERIALS AND METHODS

Force Field Parameters. All simulations were performed using the CHARMM22 protein force field[26] including the backbone dihedral cross term map (CMAP),[27] the CHARMM36 lipid force field,[28] and the TIP3P water model.[29] β_2-AR cys-314 was palmitoylated in the simulations, and the force field parameters for the thioester linkage between Cys-314 and the palmitoyl group were prepared based on the NAMD tutorial.[30] The force field parameters for ligands (carazolol, alprenolol, and BI-167107; Figure 2B) were obtained from the GAAMP (general automated atomic model parameterization) gateway, a well-validated platform for automated molecular mechanics force field parametrization.[31] All FEP/MD simulations were performed using CHARMM.[32]

Initial Structure Preparation. Initial β_2-AR models were prepared from the available crystal structures (PDB entries 2RH1, 3NYA, and 3P0G). We used preoriented coordinates with respect to the membrane normal (*Z*-axis) from OPM (orientation of protein in membranes database).[33]

β_2-AR contains a highly flexible 43-residue loop (intracellular loop 3, ICL3) between transmembrane helices 5 and 6 (Figure 2A). The original PDB structures used in this study contain T4-lysozyme (T4L) insertion that replaces 32 residues of ICL3 for the crystallographic studies.[11,34] This T4L insertion was removed in the simulations because of the experimental evidence that a split β_2-AR without ICL3 assembles to form a functional receptor.[35] The chain termini were neutralized by acetyl and methylamino neutral terminal patches. All non-protein molecules except for the palmitoyl group and ligand were removed.

In the cases where the PDB structures do not have the coordinates of the palmitoyl group (PDB entries 3NYA and 3P0G), the corresponding coordinates in PDB:2RH1 were copied to attach the palmitoyl group to Cys-314. All Lys and Arg residues were protonated, and all His, Glu, and Asp residues were deprotonated except Glu-122, which likely exists in the protonated state due to the membrane hydrophobic environment surrounding the residue.[36] Two disulfide bonds (Cys-106/191 and Cys-184/190) were added in the proteins.

For simulations of the states whose crystal structures are not available (inactive β_2-AR/BI-167107 (full agonist), active β_2-AR/carazolol (inverse agonist), and active β_2-AR/alprenolol (neutral antagonist)), initial structures were obtained by docking the corresponding ligand to the β_2-AR crystal structure of the desired state (see below). Table 1 lists the six β_2-AR/ligand systems simulated in this study with their symbolic names: superscript C for initial ligand pose taken from the crystal structure and M for those obtained by molecular docking.

Table 1. β_2-AR/Ligand Complex Systems Simulated in This Study

system	receptor PDB	receptor state	ligand PDB	ligand name	initial ligand pose
I-inv^C	2RH1	inactive	2RH1	carazolol	crystal
I-neu^C	3NYA	inactive	3NYA	alprenolol	crystal
I-ago^M	2RH1	inactive	3P0G	BI-167107	docking
A-inv^M	3P0G	active	2RH1	carazolol	docking
A-neu^M	3P0G	active	3NYA	alprenolol	docking
A-ago^C	3P0G	active	3P0G	BI-167107	crystal

Molecular Docking. Ligand conformations were first extracted from the PDB files and then randomized to avoid any bias toward the crystal binding poses. Maestro[37] was used to assign the bond orders of the ligands and to add hydrogen atoms. The ligand and receptor structures were preprocessed using Raccoon[38] for the docking experiments. AutoDock Vina[39] was used for virtual ligand docking. A cubic grid of (20 Å)^3 was placed at the geometric center of the cognate ligand in each crystal structure. The best-score docking poses were used as the initial structures for MD (equilibration) simulations for I-ago^M, A-inv^M, and A-neu ^{M} in Table 1.

System Setup and Equilibration. The prepared β_2-AR/ligand complexes were embedded into an explicit 1-palmitoyl–2-oleoyl-*sn*-glycero-3-phosphocholine (POPC) bilayer using the *Membrane Builder* module[40,41] in CHARMM-GUI.[42] 150 mM KCl was added in the solvated region for physiological salt concentration. The initial system sizes were about 75 Å × 75 Å × 85 Å. The van der Waals interactions were smoothly switched off at 10–12 Å by a force-switching function.[43] The electrostatic interactions were calculated using the particle mesh Ewald (PME) method[44] with a mesh size of ~1 Å for fast Fourier transformation, $\kappa = 0.34$ Å^{-1}, and a sixth-order B-spline interpolation. The detailed simulation system information is summarized in the Supporting Information, Table S1.

Each initial system was shortly equilibrated for 300 ps by applying various restraints to protein backbone, side-chain,

DOI: 10.1021/ct5008907
J. Chem. Theory Comput. 2015, 11, 1255–1266

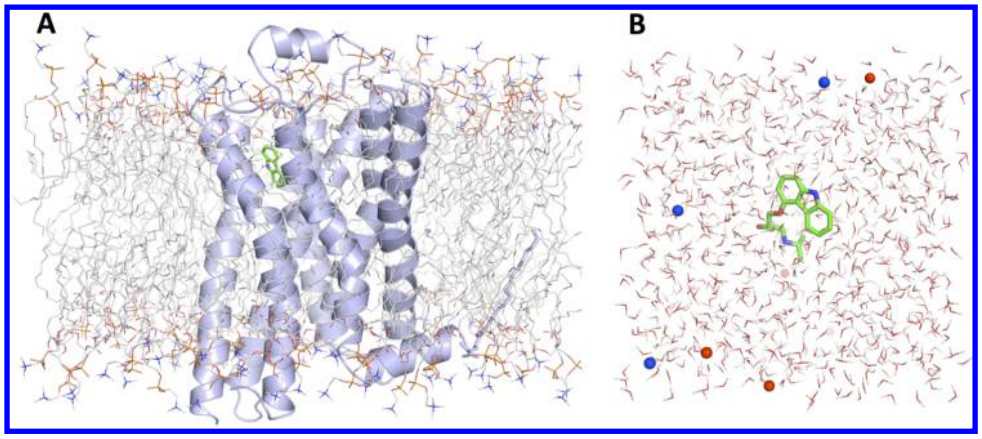

Figure 3. All-atom β_2-AR/ligand simulation systems for (A) *SITE* and (B) *BULK*. The β_2-AR structure is shown in cartoon representation, the ligand in stick representation, and lipid and water molecules in line representation. K^+ and Cl^- ions, shown as spheres, in *BULK* are colored in blue and red, respectively. In *SITE*, water and ions are not displayed for clarity. Note that the system size of *BULK* is much smaller than that of *SITE*, but the figure for BULK here is amplified for clarity.

water, ions, and lipid tail/head atoms at 303.15 K with default options in the standard 6-step *Membrane Builder* equilibration inputs. The hydrogen geometry was kept fixed using SHAKE.[45] After the short relaxation, an additional 2 ns equilibration run was performed for each system without restraints. All calculations were performed in an NPT ensemble (constant particle number, pressure, and temperature).[46] The simulation time-step was 2 fs. Figure 3 shows the last snapshots of I-inv^C for *SITE* and *BULK* systems for the FEP/MD simulations, where *SITE* represents a β_2-AR/ligand system in a fully hydrated membrane and *BULK* a ligand-only system in aqueous solution.

To prepare the *BULK* systems, ligand structures were solvated in a water box (~33 Å × 33 Å × 33 Å) with 150 mM KCl, and the solvated systems were minimized for 1,000 steps using the steepest descent method followed by 1,000 steps using the adopted basis Newton−Raphson method. NVT (constant particle number, volume, and temperature) dynamics at 300 K was performed for 200 ps to relax the water molecules and ions. Then, an additional 200 ps NPT equilibration was carried out.

FEP/MD Calculations. The FEP/MD simulation protocols were obtained from CHARMM-GUI *Ligand Binder*[47] and modified for this study. Instead of effective solvent boundary potentials to approximate the outside of a small region of interest using the continuum electrostatics,[48,49] the (fully atomistic) periodic boundary conditions (PBC) were used in both the *SITE* and *BULK* simulations. The absolute binding free energy calculations were carried out with the PERT module in CHARMM using the staged alchemical FEP/MD simulation approach with restraint potentials. The details of the theory and protocols are described elsewhere.[47,50−53] The FEP/MD simulations for each system in Table 1 consist of 137 windows including both *SITE* and *BULK* calculations. Each window was simulated for 7 ns, corresponding to 959 ns for each system.

In this study, we calculated absolute ligand binding free energies in two different ways: block-averaged (Figure 5 and Table 2) and accumulated binding free energies (Figures 6 and 7). The block-averaged binding free energies were calculated using FEP/MD results within a given simulation interval (i.e., 500 ps in this study). The accumulated binding free energies were computed from the beginning of the simulation up to a given simulation time.

Free Energy Correction by the Mean Electrostatic Potential Shift of Solvent Phase. In the staged alchemical FEP/MD simulation, the electrostatic contribution to the binding free energy is the difference between the charging free energy of the ligand in *SITE* and *BULK*. Alchemical free energy simulations for charging processes of a non-neutral ligand in a protein experience an artificial electrostatic free energy contribution due to difficulties in treating the long-range Coulomb interactions using particle mesh Ewald under periodic boundary conditions during FEP/MD simulations.[54] The three ligands used in this study (carazolol, alprenolol, and BI-167107) have a net charge of +1*e*. In our simulation systems, the mean electrostatic potential of the solvent phase is not the same in *SITE* and *BULK* due to large compensation for the positive potential in the nonsolvent phase (protein/ligand complex and membrane) in *SITE*. Such a discrepancy results in a potential shift toward a negative value compared to the solvent phase in *BULK*.[54] For a positive ligand, this potential shift makes the binding appear too favorable.

To correct this artificial potential shift, we calculated the mean electrostatic potential in the solvent phase in both *SITE* and *BULK* using the PMEPot plug[55] in VMD[56] for every window for the charging free energy calculations. The solvent potential is little affected by ligand charge perturbation and simulation time, and is close to zero in *BULK* due to a small volume fraction of each ligand. However, the solvent potential in *SITE* is significant and negative values regardless of windows (Supporting Information, Figure S1). The mean potential shift, the potential in *SITE* minus the potential in *BULK*, averaged over all the windows during 3 ns FEP/MD runs was subtracted from the electrostatic contribution.

RESULTS AND DISCUSSION

System Equilibration. Figure 4 shows the time-series of root-mean-square deviations (RMSD) of β_2-AR (red) and ligand (blue) for all the *SITE* systems during the 2 ns equilibration simulations. Both protein and ligand are very stable in all systems. We previously observed that non-native ligand poses modeled by docking show large deviations (generally more than 2 Å RMSD) during short equilibration simulations.[53] In this study, all systems started from model

DOI: 10.1021/ct5008907
J. Chem. Theory Comput. 2015, 11, 1255−1266

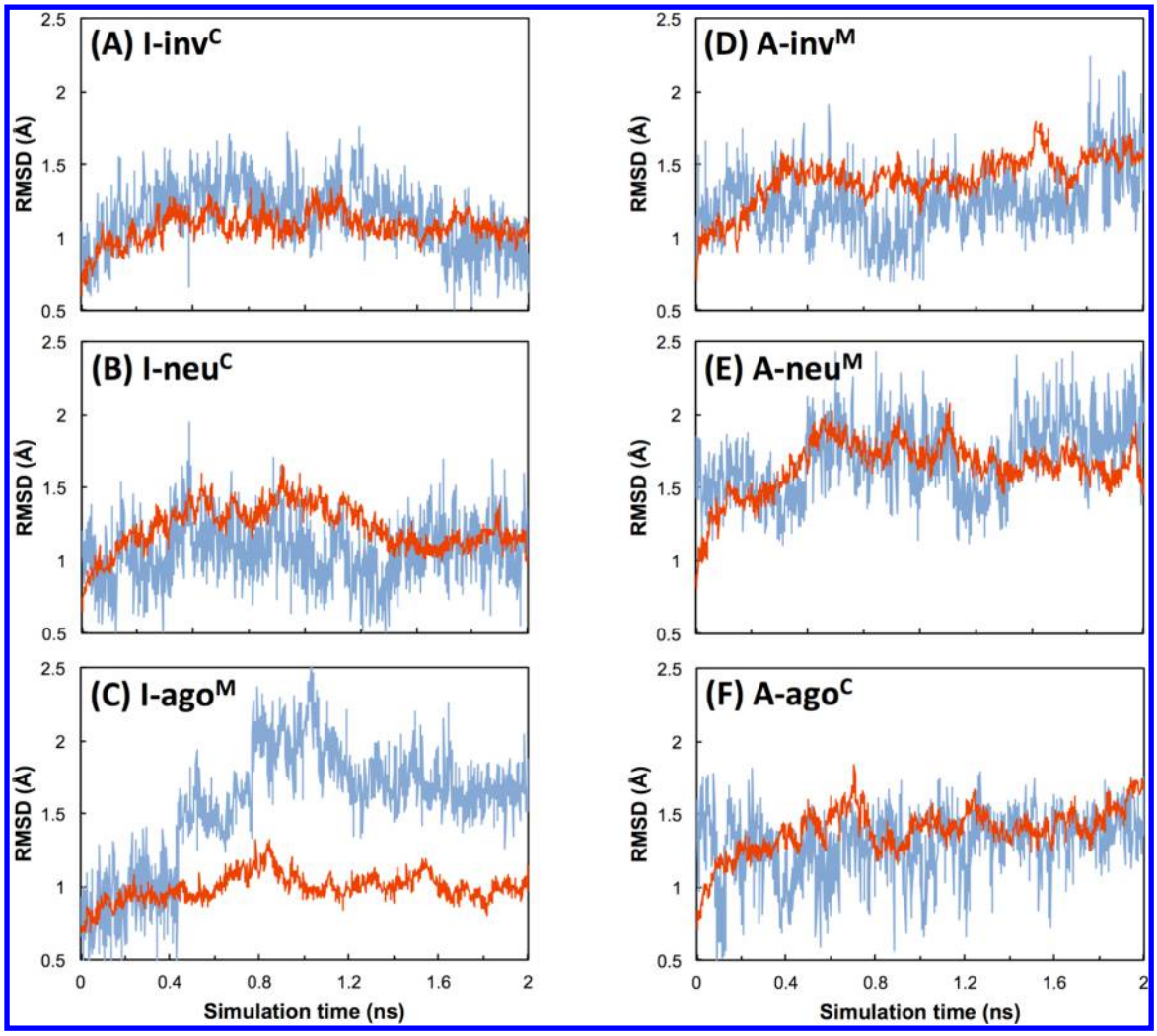

Figure 4. Equilibration of the *SITE* systems. RMSDs were calculated from the initial structures using Cα atoms in the protein (red) and heavy atoms in the ligand (blue).

structures (I-ago^M, A-inv^M, and A-neu^M) remain stable with the average RMSDs less than 2 Å during the last 500 ps, implying that the predicted ligand poses represent stable states.

For the active β_2-AR systems, we used a crystal structure of agonist-bound β_2-AR (A-ago^C) in which the receptor is stabilized by a G-protein-mimetic nanobody, but the nanobody is absent in our simulation systems. The systems with active β_2-AR consistently show larger fluctuations of β_2-AR RMSD than in the corresponding inactive β_2-AR systems; the average RMSDs of β_2-AR during the last 500 ps of the equilibration are 1.06 ± 0.07 Å (I-inv^C), 1.13 ± 0.06 Å (I-neu^C), and 0.99 ± 0.07 Å (I-ago^M) for inactive β_2-AR and 1.55 ± 0.10 Å (A-inv^M), 1.65 ± 0.08 Å (A-neu^M), and 1.48 ± 0.09 Å (A-ago^C) for active β_2-AR. This is consistent with previous observations[16] that the active state without an intracellular binding partner is less stable than the inactive state, although the current 2 ns equilibration is not long enough to sample a large conformational space for β_2-AR.

Comparison of Calculated Absolute Binding Free Energies to Experimental Data. The alchemical FEP/MD simulations started from the last snapshots of the equilibration simulations. Figure 5A shows the change of the 500 ps block-averaged binding free energies as a function of simulation time for the three systems based on the crystal structures (I-inv^C, I-neu^C, and A-ago^C). The average of the last 3 ns was used for comparison with experimental measurements in Figure 5B. The experimental values were taken from refs 12, 57, and 58. Overall, ligand binding free energies from the calculations are not largely different from the experimental measurements. However, the free energy of I-inv^C is less favorable than the experimental value, while those of I-neu^C and A-ago^C are more favorable. The discrepancy may arise from the fact that the simulations cannot sufficiently sample the conformational space of the protein. Vilardaga et al. applied fluorescence-based techniques for real-time monitoring of the activation of two GPCRs in living cells: the α2A-adrenergic receptor (α2A-AR) and the parathyroid hormone receptor (PTHR). They observed ~40 ms for α2A-AR and ~1 s for PTHR.[59] Certainly, our 7 ns FEP/MD simulation is too short to sample the dynamics and conformational changes of β_2-AR that requires milliseconds or more. Despite this limitation, the current simulation still provides useful information on differences in the binding events of ligands with varying efficacy, as described in the next subsections. There have been advanced free energy sampling schemes and FEP/MD methodologies such as the orthogonal space sampling strategy[60] and free energy perturbation Hamiltonian replica-exchange MD (FEP/H-REMD),[61] respectively. Incorporation of these approaches

DOI: 10.1021/ct5008907
J. Chem. Theory Comput. 2015, 11, 1255−1266

could improve the efficiency in sampling the conformation of highly dynamic receptors like GPCRs for accurate ligand binding free energy calculations.

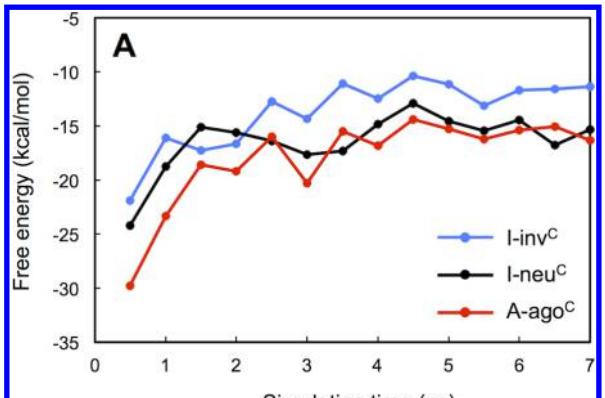

B

System	ΔG_b°	Exp
I-inv^C	−11.56 ± 0.91	−13.65
I-neu^C	−14.92 ± 1.29	−12.41
A-ago^C	−15.45 ± 0.72	−13.83

Figure 5. Absolute ligand binding free energy calculated for the crystal structure systems. (A) Change in the 500 ps block-averaged free energy as a function of simulation time. (B) Comparison with the experimental results. The average (± standard deviation) of the last 3 ns was used as the calculated binding free energies.

In addition to β_2-AR conformational sampling, there could be other factors that can influence the energy landscape of ligand-bound β_2-AR. In experiments, there are protein−protein interactions by GPCR oligomerization or by binding of other membrane proteins or intracellular partners, which are missing in our simulations. In addition, we used only POPC lipids to build the membrane bilayer, yet different composition of diverse lipids may modulate the receptor dynamics. Finally, inaccuracy of the force field that we used for the free energy simulations could be a factor. For these reasons, calculating accurate binding free energies of GPCR ligands is still computationally challenging.

Discrimination of Ligand Efficacy Characterized by Free Energy Calculations. A major aim of our FEP/MD simulations is to explore the possibility of using these relatively short FEP/MD simulations to computationally discriminate the efficacy of the GPCR ligands. Figure 6 plots the accumulated binding free energy as a function of simulation time. The accumulated free energies up to 3 ns are shown to make a clear comparison of the free energy changes during the early stage of FEP/MD simulations. A common feature is that the free energy becomes unfavorable rapidly during the first 500 ps simulations. Such rapid changes arise from the conformational adaptation of the receptor by alchemical annihilation of the ligand, such as rearrangement of highly flexible side-chains within the ligand binding site, and then the binding free energy gradually increases by slow shift of other movable parts as the simulation goes on. Strikingly, only the neutral antagonist-bound inactive β_2-AR complex (I-neu^C: black line in Figure 6A) does not show the rapid change in the free energy at the early stage of the FEP/MD simulation, which can be used as a characteristic for neutral antagonist efficacy.

To analyze why I-neu^C shows such a different convergence behavior from I-inv^C, the accumulated free energy of I-neu^C and I-inv^C in Figure 6 are further analyzed and compared. Figure 7 shows the time-series of the interaction free energy in *SITE* and *BULK*, and its decomposed free energy contributions in *SITE* for I-neu^C (black) and I-inv^C (blue). The *BULK* simulations converge quickly, while the interaction free energy in *SITE* becomes unfavorable rapidly (with a sharp increase in I-inv^C). The rapid change of the interaction free energy during the first 500 ps simulations is mainly associated with significant increase in the repulsive and electrostatic contributions as well as slight decrease in the dispersive contribution. In the case of I-neu^C, the relaxation of the strain energy (introduced by ligand binding) in the binding-site conformation is not significant compared to I-inv^C (see the subsection Molecular Basis of Ligand Efficacy below). This behavior of I-neu^C observed upon the alchemical perturbation of the free energy simulations is consistent with the expectation that binding of neutral antagonist does not greatly affect the static and dynamic features of the binding site.

As shown in Figure 6A, the overall shape of the free energy curves for I-inv^C (blue) and I-ago^M (red) are a little different, although the overall free energy change in I-ago^M is larger. The decomposition to the individual free energy contributions also provides valuable insights into such receptor−ligand interactions. Table 2 shows the averaged free energy components calculated using 500 ps block-averaged free energies. The repulsive free energy is much more unfavorable in I-ago^M, whereas its dispersive free energy is relatively comparable to those of I-inv^C and I-neu^C. The absolute ratios of the dispersive free energy to the repulsive free energy are 1.75 (I-inv^C), 1.92 (I-neu^C), and 1.24 (I-ago^M). These physical properties characterized by free energy simulations provide valuable insights into β_2-AR ligand efficacy discrimination, which is hard to obtain from conventional binding affinity experiments or molecular docking simulations. In other words, a neutral antagonist (I-neu^C) shows no rapid change in the binding free energy at the early stage of the FEP/MD simulation, while an inverse agonist (I-inv^C) shows a larger strain energy (i.e., tighter fit into the binding site) than a neutral antagonist, and a full agonist (I-ago^M) shows a larger repulsive free energy than a neutral antagonist and an inverse agonist in inactive β_2-AR. The data also suggest that even FEP/MD simulations only with an inactive β_2-AR conformation provide reliable information to discriminate three different ligand efficacies.

A comparison of the free energy simulation results from inactive β_2-AR with those from active one can provide additional properties for more accurate discrimination of ligand efficacy. A prominent feature discriminating a full agonist from an inverse agonist and a neutral antagonist in the free energy simulations is that full agonist-bound β_2-AR is the only system showing higher affinity to active β_2-AR (A-ago^C) than inactive one (I-ago^M), whereas both inverse agonist and neutral antagonist show less favorable binding free energy in the active β_2-AR state (Table 2). The dispersion free energy of the full agonist becomes significantly more favorable when the ligand is in active β_2-AR (A-ago^C) than in inactive one (I-ago^M), but other ligands show an opposite tendency (Table 2). On the other hand, neutral antagonist-bound β_2-AR shows the smallest affinity difference in both receptor conformations, which can be used to discriminate a neutral antagonist from others.

DOI: 10.1021/ct5008907
J. Chem. Theory Comput. 2015, 11, 1255−1266

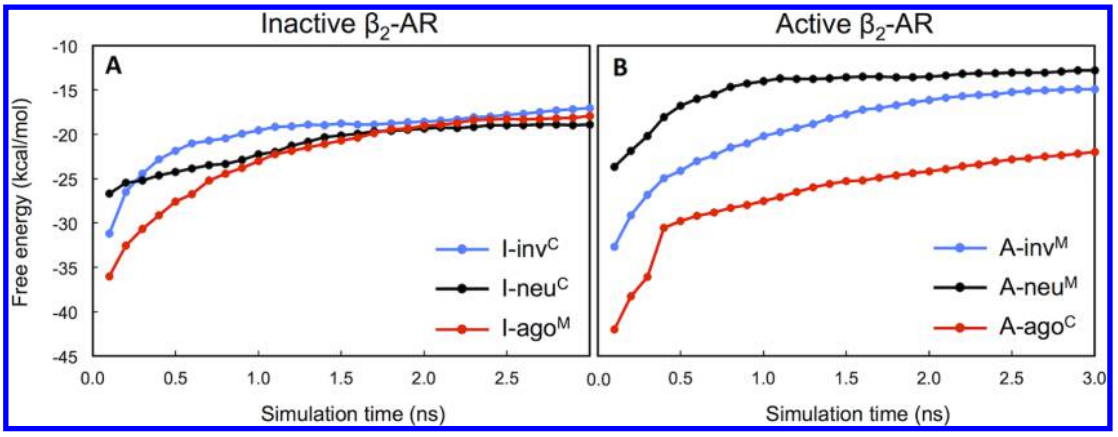

Figure 6. Discrimination of β_2-AR ligand efficacy by absolute ligand binding free energy calculations. The cumulated free energies are plotted as a function of simulation time.

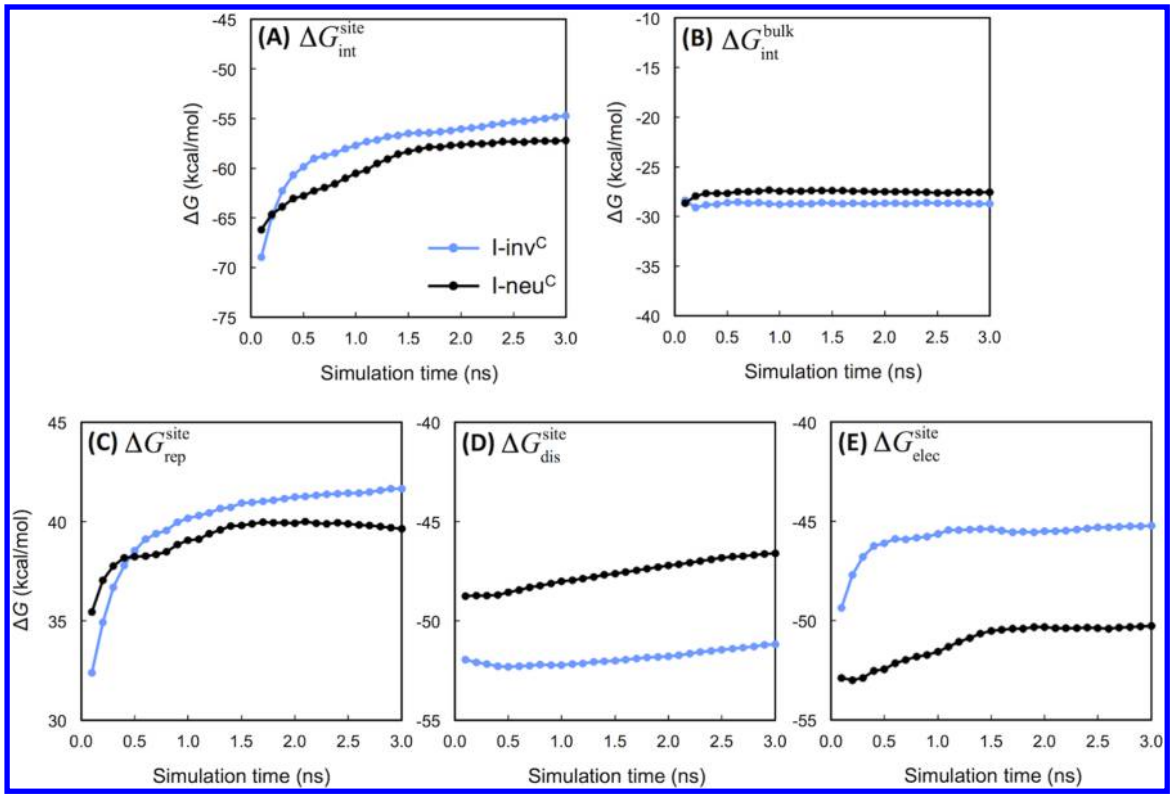

Figure 7. Comparison of the decomposed free energies between I-neu^C (black) and I-inv^C (blue) from Figure 6A. ΔG_{int} is the interaction free energy and can be decomposed into the repulsive (ΔG_{rep}), dispersive (ΔG_{dis}), and electrostatic (ΔG_{elec}) contributions.

Table 2. Free Energy Decomposition[a]

	repulsion	dispersion	electrostatics	interaction	trans/rot	conf	total
I-inv^C	9.00	−15.73	−13.66	−20.39	5.92	2.91	−11.56
I-neu^C	7.82	−15.04	−17.38	−24.60	6.39	3.30	−14.92
I-ago^M	14.83	−18.37	−21.33	−24.87	6.68	5.46	−12.73
A-inv^M	13.03	−15.29	−14.61	−16.87	5.91	2.10	−8.86
A-neu^M	7.65	−12.90	−13.59	−18.84	4.75	0.80	−13.30
A-ago^C	17.60	−22.55	−20.56	−25.52	7.02	3.05	−15.45

[a]The absolute binding free energy and its decomposed contributions (kcal/mol) are listed for all the systems. "trans/rot" and "conf" are the free energy cost associated with the loss of the translational/rotational and conformational degrees of freedom of ligand upon binding, respectively. 500 ps block-averaged free energies were calculated (up to 7 ns) and the average of the last 3 ns was used as the values in the table. The standard deviations (about 4-8% of each component) are not displayed for clarity.

DOI: 10.1021/ct5008907
J. Chem. Theory Comput. 2015, 11, 1255−1266

Ligand Specificity to Different Activation States of β_2-AR. An intriguing feature observed in the last column of Table 2 is the binding affinity difference of the ligands to the active and inactive conformations of β_2-AR. Like many GPCRs, it has been experimentally characterized that β_2-AR has two agonist affinity states:[16,62] a low-affinity state in the absence of cognate G protein (i.e., resulting from agonist binding to more populated inactive states) and a high-affinity state in the presence of G protein.[16,57] This result indicates that agonists bind more tightly to the active β_2-AR conformation than to the inactive one, so that agonist binding shifts the equilibrium of the ligand binding site (and thus the receptor conformation) toward the active state. These experimental evidence are in qualitative agreement with the current results on the binding affinities that are dependent on the activation states of the receptor.

This ligand specificity may also be studied by cognate and noncognate receptor docking experiments (Table 3). Cognate docking accurately reproduced the native poses for all ligands. When the active conformation was used, the docking pose of the inverse agonist showed a large deviation from the binging pose in I-inv^C (9.46 Å RMSD, Supporting Information, Figure S2). While structural changes in the ligand binding pocket upon β_2-AR activation are relatively subtle (Figure 2C), the inward movement of transmembrane helices 5, 6, and 7 interferes with binding of the inverse agonist,[12] resulting in steric clashes if the inverse agonist would be transferred to the binding site of the active conformation (Supporting Information, Figure S3). While distinction of an inverse agonist may be possible by these docking results due to the structural incompatibility of an inverse agonist with the active receptor conformation, discrimination between neutral antagonist and agonist may be less clear due to smaller changes in docking poses and inaccuracy of predicted binding affinities. For example, the smallest difference between the predicted binding affinities to the active and inactive receptor conformations is only 0.5 kcal/mol for the agonist. The corresponding value obtained from the FEP/MD simulations is 2.72 kcal/mol, which show clearly different discrimination for agonist.

Table 3. Comparison of Docking Poses and Docking Scores[a]

		receptor structure		
		I-inv^C	I-neu^C	A-ago^C
ligand structure	I-inv^C	0.94 (−10.0)	1.17 (−8.9)	9.46 (−8.5)
	I-neu^C	1.09 (−7.8)	0.53 (−7.7)	2.18 (−7.4)
	A-ago^C	1.07 (−10.1)	1.81 (−10.3)	1.49 (−10.8)

[a]Heavy atom RMSDs (Å) between the docked and crystal ligand poses are given in the table with docking scores (kcal/mol) in parentheses. The best score docking poses were used for the RMSD measurement. In the case of non-cognate docking, the RMSDs were calculated based on the superposed structures of native ligand bound-receptor onto non-cognate target receptor.

Molecular Basis of Ligand Efficacy. The molecular basis of ligand efficacy is further elucidated using the inactive β_2-AR bound with the inverse agonist, neutral antagonist, and full agonist. The inactive β_2-AR is chosen because the inverse agonist is difficult to bind to the active β_2-AR conformation, as illustrated in molecular docking (Table 3 and Supporting Information, Figures S2−S3). First, the number of heavy atom contacts between β_2-AR and each ligand is compared for I-inv^C, I-neu^C, and I-ago^M during the FEP/MD simulations in $\lambda_{rep} = \lambda_{dis} = \lambda_{elec} = 1$, where λ_{rep}, λ_{dis}, and λ_{elec} are the alchemical coupling parameters for the repulsive, dispersive, and electrostatic interactions between β_2-AR and each ligand. Figure 8A,C show the time-series of the contact number. The residue-based differences in the number of contacts were also calculated between I-inv^C and I-neu^C (Figure 8B) and between I-inv^C and I-ago^M (Figure 8D). For structural comparison, frequent contact residues identified in Figure 8B,D are illustrated in Figure 9. Below, based on these results together with all other analyses performed in this study, we elaborate the underlying molecular basis of ligand efficacy in detail.

Alprenolol, a neutral antagonist, interacts less closely with the binding site residues than Carazolol, an inverse agonist, in the inactive receptor (Figure 8A; the average number of contacts during the last 3 ns is 71.53 ± 9.11 for the inverse agonist and 64.23 ± 6.62 for the neutral antagonist), whereas the interaction free energy of alprenolol is more favorable due to more favorable electrostatic interactions (Table 2). When we define "key residues" by six binding-site residues (Tyr-199, Ala-200, Ser-203, Ser-207, Trp-286, and Tyr-308) which show the largest displacement upon activation (i.e., based on PDB:2RH1 (inactive) and PDB:3P0G (active)), any of these key residues do not belong to more frequently contacting residues in I-neu^C (Figure 9A). Alprenolol's lower contacts to the binding-site residues, especially the key residues, allow relatively less restricted movements of the binding site residues, compared to the case of I-inv^C. This low strain energy of the binding site residues is reflected by the free energy curve that does not show a rapid increase within the early stage of the simulations (Figure 6A). These receptor−ligand interaction patterns are attributed to alprenolol's reduced bulkiness as well as the absence of hydrogen bond forming groups at a substructure corresponding to the heterocycle of carazolol (Figure 2B). These weak interactions with the key residues do make little impacts on stabilization or destabilization of the receptor conformation. In addition, alprenolol shows similar binding affinities in both receptor conformations (Table 2), compared to other ligands, indicating a little preference of alprenolol for either inactive or active state. These features make alprenolol a neutral antagonist.

Carazolol, an inverse agonist, fits optimally within the binding pocket of inactive β_2-AR (Tables 2 and 3). Carazolol cannot bind properly in active β_2-AR due to steric hindrance in the binding pocket (Supporting Information, Figures S2−S3), suggesting little effect on stability of the active β_2-AR state. The binding of carazolol in the inactive β_2-AR conformation stabilizes the state, i.e., eventually increasing the population of the inactive conformation and thus lowering the basal activity, which makes carazolol an inverse agonist.

BI-167107, a full agonist, can bind to inactive and active binding site in similar poses (Table 3). However, BI-167107 can optimally bind to the active β_2-AR conformation (Table 2), resulting in stabilizing the active state. Less favorable binding to the inactive β_2-AR conformation destabilizes the inactive state and shifts the equilibrium toward the active state, which makes BI-167107 a full agonist. Based on a comparison of the ligand structures (Figure 2B) and the docking results (Table 3), it is clear that BI-167107 has shorter linker between heterocycle and the amine that interacts with Asp$^{3.32}$ than carazolol. Nevertheless, BI-167107 makes more contacts with the binding site residues in inactive β_2-AR than carazolol (Figure 8C; the average number of contacts is 87.17 ± 8.37 for the full agonist)

DOI: 10.1021/ct5008907
J. Chem. Theory Comput. 2015, 11, 1255−1266

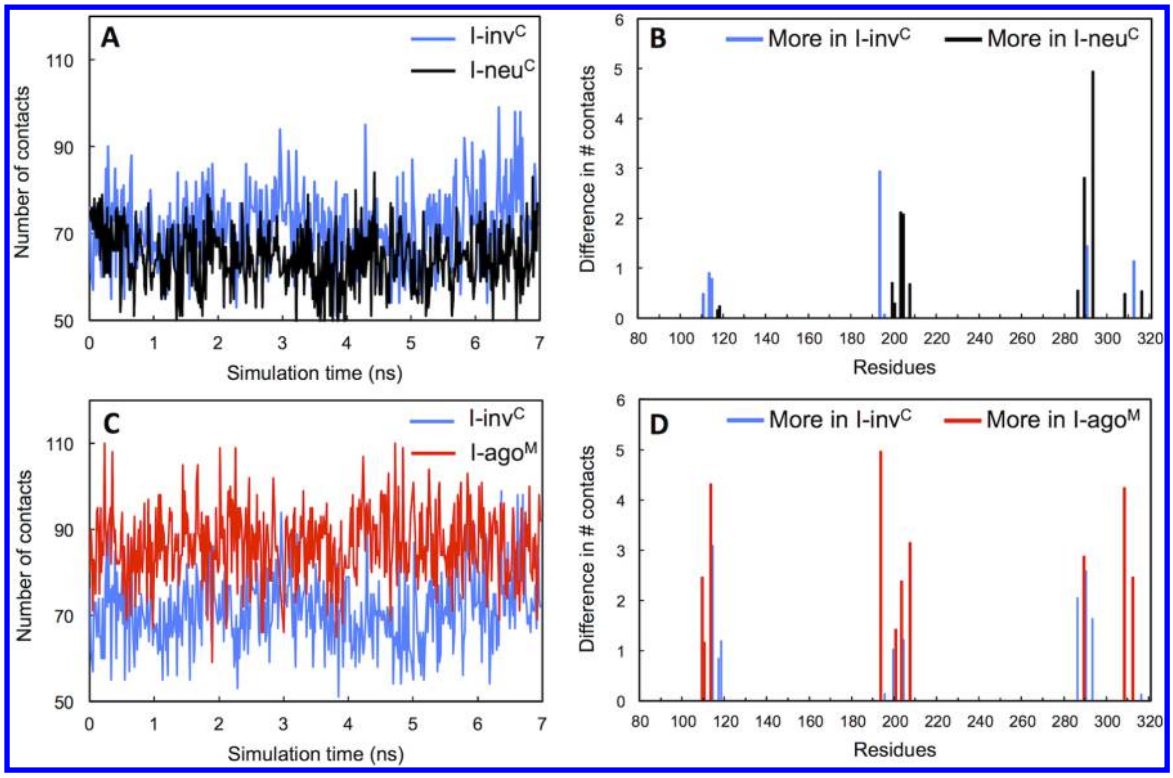

Figure 8. Number of contacts between β_2-AR and ligand during the simulation. The measurement was performed for the FEP/MD state with intact interactions between the receptor and ligand ($\lambda_{rep} = \lambda_{dis} = \lambda_{elec} = 1$). The contact was defined by a distance cutoff of 4 Å between heavy atoms. (A and C) The time-series of the number of contacts for I-inv^C (blue), I-neu^C (black), and I-ago^M (red). (B and D) The difference of the average number of contacts as a function of residue number. The average values were calculated using the last 3 ns simulation production. The binding site residues were defined by a distance cutoff of 4.5 Å between receptor and ligand heavy atoms in I-inv^C.

because of additional functional groups for hydrogen bonds in the heterocycle as well as a longer alkyl phenyl ring substituent on the amine group. As shown in a superposed structure of the native pose of carazolol and the docking pose of BI-167107 in inactive β_2-AR (Supporting Information, Figure S4), the distance between the hydroxyl group of Ser-203 and the nitrogen atom of the heterocycle in BI-167107 is longer than that for carazolol, indicating that a movement of BI-167107 toward transmembrane helix 5 is required to form a stable hydrogen bond. Nonetheless, as mentioned above, the atom contact analysis shows that BI-167107 interacts more strongly with Ser-203 (Figures 8D and 9B). This indicates that a readjustment of BI-167107 toward transmembrane helix 5 easily occurs in the binding pocket of inactive β_2-AR. It is likely that the longer alkyl substituent will not only provide higher binding affinity but also play a role as an effective anchor to position the full agonist to its native location after hydrogen bond formation, resulting in a pulling effect to cause the inward movement of transmembrane helix 5.

CONCLUSIONS

GPCR-mediated signaling can be modulated by ligands (agonist, inverse agonist, and neutral antagonist), which is termed ligand efficacy. Accurate characterization of the ligand efficacy is a critical factor to develop highly effective GPCR drugs. In this study, we have presented a FEP/MD simulation study in explicit membranes to explore a molecular basis of β_2-AR ligand efficacy for a representative inverse agonist (carazolol), neutral antagonist (alprenolol), and full agonist (BI-167107), aiming to bridge the gap between simple docking calculations and highly expensive millisecond-timescale MD simulations. Our study demonstrates that relatively short free energy calculations (for each window) provide relevant physical properties to discriminate β_2-AR ligand efficacy. A neutral antagonist, alprenolol, is the only ligand whose binding free energy in inactive β_2-AR is little affected by the rearrangement of the binding site residues during the alchemical simulations, due to less perturbation to the binding pocket by alprenolol, in particular to the residues mainly involved in receptor activation. A full agonist, BI-167107, is the only ligand whose binding affinity is stronger in the active β_2-AR, indicating its role in stabilizing the active state. BI-167107 can bind to both inactive and active β_2-AR in a similar pose but shows much more unfavorable repulsive free energy contribution in inactive β_2-AR due to its lower fitness, compared to better fitness of an inverse agonist, carazolol. This less fitness destabilizes the inactive β_2-AR and consequently shifts the conformational equilibrium toward the active state.

Although our study is focused only on β_2-AR, the current computational approach and the concept to interpret the results, which are summarized in the following, can be applied to most GPCRs if not all. Given a target GPCR whose crystal or modeled active conformation is available, an initial complex structure for a given ligand can be generated using molecular docking. After proper equilibration of the initial GPCR/ligand structure, FEP/MD simulations are performed for 5 ns at least to ensure the simulation convergence. Analysis of the time-series of ligand binding free energies during the first 1 ns and the last 1 ns, and the free energy decomposition of the last 1 ns may provide reliable physical descriptors on ligand efficacy as well as affinity. If both active and inactive conformations of the

DOI: 10.1021/ct5008907
J. Chem. Theory Comput. 2015, 11, 1255−1266

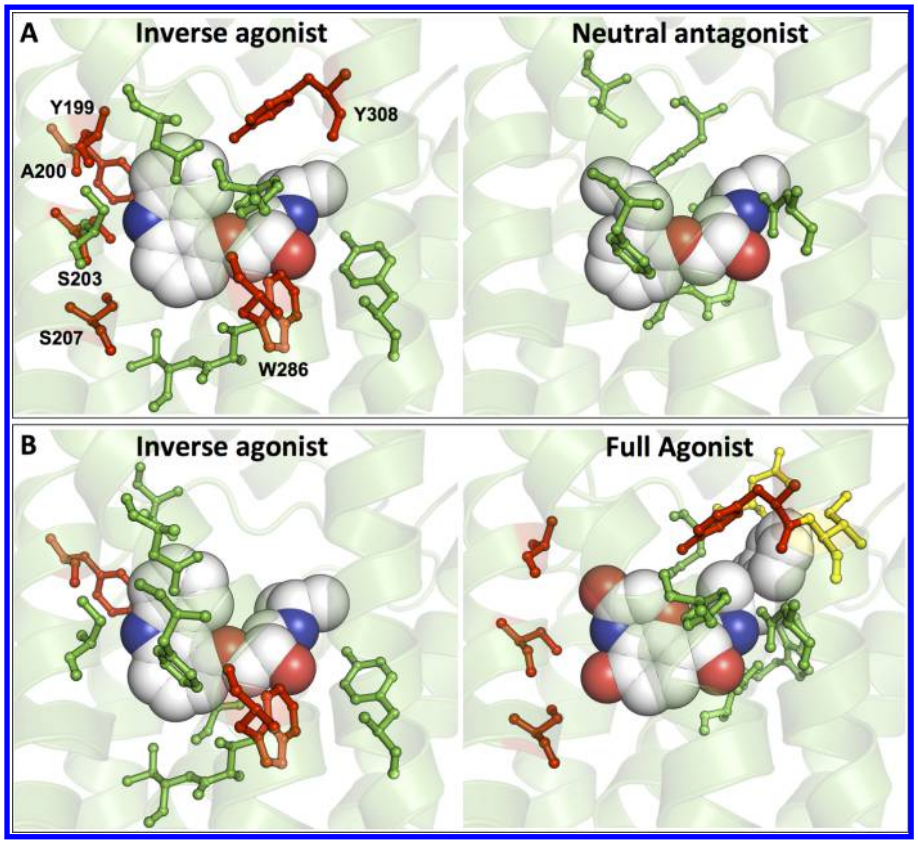

Figure 9. Structural illustration of the residues with more contacts identified in Figure 8B,D. (A) Comparison between I-inv^C and I-neu^C. (B) Comparison between I-inv^C and I-ago^M. The β_2-AR residues showing relatively large movement during the activation (>0.8 Å Cα-Cα distance) are colored in red. The distances were measured between β_2-AR structures in PDB:2RH1 and PDB:3P0G. In the full agonist figure of (B), the residues that are additionally defined on the basis of I-ago^M are also displayed in yellow.

target GPCR are available, a comparison of the free energy simulation results from both states could provide additional information for more accurate discrimination of ligand efficacy. The results on ligand poses and affinities from the docking experiments could be used to compliment the FEP/MD results. It is our hope that our computational approach improves research and development efficiency in designing novel lead compounds targeting various GPCRs for the treatment of various human diseases.

■ ASSOCIATED CONTENT

Supporting Information

Simulation system information. Mean electrostatic potential in solvent phase for system I-inv^C. Docking pose of inverse agonist in active β_2-AR conformation. Structural difference of the ligand binding site between inactive and active β_2-AR conformations. Superposed structure of the native pose of inverse agonist and the docking pose of full agonist in inactive β_2-AR conformation. This material is available free of charge via the Internet at http://pubs.acs.org.

■ AUTHOR INFORMATION

Corresponding Author

*E-mail: wonpil@ku.edu. Phone: (+1) 785-864-1993. Fax: (+1) 785-864-5558.

Author Contributions

The manuscript was written through contribution of all authors. All authors have given approval to the final version of the manuscript.

Notes

The authors declare no competing financial interest.

■ ACKNOWLEDGMENTS

This work was supported by NIH U54GM087519 and XSEDE MCB070009 (to W.I.) and NRF 2013R1A2A1A09012229 (to C.S.).

■ REFERENCES

(1) Deupi, X.; Kobilka, B. K. Energy landscapes as a tool to integrate GPCR structure, dynamics, and function. *Physiology (Bethesda)* **2010**, *25*, 293−303.
(2) Heilker, R.; Wolff, M.; Tautermann, C. S.; Bieler, M. G-protein-coupled receptor-focused drug discovery using a target class platform approach. *Drug Discovery Today* **2009**, *14*, 231−240.
(3) Lundstrom, K. Latest development in drug discovery on G protein-coupled receptors. *Curr. Protein Pept. Sci.* **2006**, *7*, 465−470.
(4) Overington, J. P.; Al-Lazikani, B.; Hopkins, A. L. How many drug targets are there? *Nat. Rev. Drug Discovery* **2006**, *5*, 993−996.
(5) Kenakin, T. Efficacy at G-protein-coupled receptors. *Nat Rev. Drug Discovery* **2002**, *1*, 103−110.
(6) Kobilka, B. K.; Deupi, X. Conformational complexity of G-protein-coupled receptors. *Trends Pharmacol. Sci.* **2007**, *28*, 397−406.
(7) Lefkowitz, R. J.; Shenoy, S. K. Transduction of receptor signals by β-arrestins. *Science* **2005**, *308*, 512−517.
(8) Perez, D. M.; Karnik, S. S. Multiple signaling states of G-protein-coupled receptors. *Pharmacol. Rev.* **2005**, *57*, 147−161.
(9) Hein, L.; Kobilka, B. K. Adrenergic receptor signal transduction and regulation. *Neuropharmacology* **1995**, *34*, 357−366.

DOI: 10.1021/ct5008907
J. Chem. Theory Comput. 2015, 11, 1255−1266

(10) Rosenbaum, D. M.; Rasmussen, S. G.; Kobilka, B. K. The structure and function of G-protein-coupled receptors. *Nature* **2009**, *459*, 356−363.
(11) Rosenbaum, D. M.; Cherezov, V.; Hanson, M. A.; Rasmussen, S. G.; Thian, F. S.; Kobilka, T. S.; Choi, H. J.; Yao, X. J.; Weis, W. I.; Stevens, R. C.; Kobilka, B. K. GPCR engineering yields high-resolution structural insights into β_2-adrenergic receptor function. *Science* **2007**, *318*, 1266−1273.
(12) Rasmussen, S. G.; Choi, H. J.; Fung, J. J.; Pardon, E.; Casarosa, P.; Chae, P. S.; Devree, B. T.; Rosenbaum, D. M.; Thian, F. S.; Kobilka, T. S.; Schnapp, A.; Konetzki, I.; Sunahara, R. K.; Gellman, S. H.; Pautsch, A.; Steyaert, J.; Weis, W. I.; Kobilka, B. K. Structure of a nanobody-stabilized active state of the β_2 adrenoceptor. *Nature* **2011**, *469*, 175−180.
(13) Rasmussen, S. G.; DeVree, B. T.; Zou, Y.; Kruse, A. C.; Chung, K. Y.; Kobilka, T. S.; Thian, F. S.; Chae, P. S.; Pardon, E.; Calinski, D.; Mathiesen, J. M.; Shah, S. T.; Lyons, J. A.; Caffrey, M.; Gellman, S. H.; Steyaert, J.; Skiniotis, G.; Weis, W. I.; Sunahara, R. K.; Kobilka, B. K. Crystal structure of the β_2 adrenergic receptor-Gs protein complex. *Nature* **2011**, *477*, 549−555.
(14) Nygaard, R.; Zou, Y.; Dror, R. O.; Mildorf, T. J.; Arlow, D. H.; Manglik, A.; Pan, A. C.; Liu, C. W.; Fung, J. J.; Bokoch, M. P.; Thian, F. S.; Kobilka, T. S.; Shaw, D. E.; Mueller, L.; Prosser, R. S.; Kobilka, B. K. The dynamic process of β_2-adrenergic receptor activation. *Cell* **2013**, *152*, 532−542.
(15) Kim, T. H.; Chung, K. Y.; Manglik, A.; Hansen, A. L.; Dror, R. O.; Mildorf, T. J.; Shaw, D. E.; Kobilka, B. K.; Prosser, R. S. The role of ligands on the equilibria between functional States of a g protein-coupled receptor. *J. Am. Chem. Soc.* **2013**, *135*, 9465−9474.
(16) Rosenbaum, D. M.; Zhang, C.; Lyons, J. A.; Holl, R.; Aragao, D.; Arlow, D. H.; Rasmussen, S. G.; Choi, H. J.; Devree, B. T.; Sunahara, R. K.; Chae, P. S.; Gellman, S. H.; Dror, R. O.; Shaw, D. E.; Weis, W. I.; Caffrey, M.; Gmeiner, P.; Kobilka, B. K. Structure and function of an irreversible agonist - β_2 adrenoceptor complex. *Nature* **2011**, *469*, 236−240.
(17) Gether, U.; Lin, S.; Kobilka, B. K. Fluorescent labeling of purified β_2 adrenergic receptor. Evidence for ligand-specific conformational changes. *J. Biol. Chem.* **1995**, *270*, 28268−28275.
(18) Weiland, G. A.; Minneman, K. P.; Molinoff, P. B. Fundamental difference between the molecular interactions of agonists and antagonists with the β-adrenergic receptor. *Nature* **1979**, *281*, 114−117.
(19) Contreras, M. L.; Wolfe, B. B.; Molinoff, P. B. Thermodynamic properties of agonist interactions with the beta adrenergic receptor-coupled adenylate cyclase system. I. High- and low-affinity states of agonist binding to membrane-bound β adrenergic receptors. *J. Pharmacol. Exp. Ther.* **1986**, *237*, 154−164.
(20) Borea, P. A.; Varani, K.; Gessi, S.; Gilli, P.; Dalpiaz, A. Receptor binding thermodynamics as a tool for linking drug efficacy and affinity. *Farmaco* **1998**, *53*, 249−254.
(21) Gilli, P.; Gilli, G.; Borea, P. A.; Varani, K.; Scatturin, A.; Dalpiaz, A. Binding thermodynamics as a tool to investigate the mechanisms of drug-receptor interactions: thermodynamics of cytoplasmic steroid/nuclear receptors in comparison with membrane receptors. *J. Med. Chem.* **2005**, *48*, 2026−2035.
(22) Toll, L.; Pajak, K.; Plazinska, A.; Jozwiak, K.; Jimenez, L.; Kozocas, J. A.; Tanga, M. J.; Bupp, J. E.; Wainer, I. W. Thermodynamics and docking of agonists to the β_2-adrenoceptor determined using [(3)H](R,R′)-4-methoxyfenoterol as the marker ligand. *Mol. Pharmacol.* **2012**, *81*, 846−854.
(23) Katritch, V.; Cherezov, V.; Stevens, R. C. Structure-function of the G protein-coupled receptor superfamily. *Annu. Rev. Pharmacol. Toxicol.* **2013**, *53*, 531−556.
(24) Malmstrom, R. D.; Watowich, S. J. Using free energy of binding calculations to improve the accuracy of virtual screening predictions. *J. Chem. Inf. Model.* **2011**, *51*, 1648−1655.
(25) Kohlhoff, K. J.; Shukla, D.; Lawrenz, M.; Bowman, G. R.; Konerding, D. E.; Belov, D.; Altman, R. B.; Pande, V. S. Cloud-based simulations on Google Exacycle reveal ligand modulation of GPCR activation pathways. *Nat. Chem.* **2014**, *6*, 15−21.
(26) MacKerell, A. D.; Bashford, D.; Bellott, M.; Dunbrack, R. L.; Evanseck, J. D.; Field, M. J.; Fischer, S.; Gao, J.; Guo, H.; Ha, S.; Joseph-McCarthy, D.; Kuchnir, L.; Kuczera, K.; Lau, F. T. K.; Mattos, C.; Michnick, S.; Ngo, T.; Nguyen, D. T.; Prodhom, B.; Reiher, W. E.; Roux, B.; Schlenkrich, M.; Smith, J. C.; Stote, R.; Straub, J.; Watanabe, M.; Wiorkiewicz-Kuczera, J.; Yin, D.; Karplus, M. All-atom empirical potential for molecular modeling and dynamics studies of proteins. *J. Phys. Chem. B* **1998**, *102*, 3586−3616.
(27) Mackerell, A. D., Jr.; Feig, M.; Brooks, C. L., 3rd Extending the treatment of backbone energetics in protein force fields: limitations of gas-phase quantum mechanics in reproducing protein conformational distributions in molecular dynamics simulations. *J. Comput. Chem.* **2004**, *25*, 1400−1415.
(28) Klauda, J. B.; Venable, R. M.; Freites, J. A.; O'Connor, J. W.; Tobias, D. J.; Mondragon-Ramirez, C.; Vorobyov, I.; MacKerell, A. D., Jr.; Pastor, R. W. Update of the CHARMM all-atom additive force field for lipids: validation on six lipid types. *J. Phys. Chem. B* **2010**, *114*, 7830−7843.
(29) Jorgensen, W. L.; Chandrasekhar, J.; Madura, J. D.; Impey, R. W.; Klein, M. L. Comparison of simple potential functions for simulating liquid water. *J. Chem. Phys.* **1983**, *79*, 926−935.
(30) Amaro, R.; Dhaliwal, B.; Luthey-Schulten, Z. Developing topology and parameter files. http://www.ks.uiuc.edu/Training/Tutorials/science/forcefield-tutorial/forcefield-html/node6.html (accessed 08/16/2013).
(31) Huang, L.; Roux, B. Automated force field parameterization for nonpolarizable and polarizable atomic models based on ab initio target data. *J. Chem. Theory. Comput.* **2013**, *9*, 3543−3556.
(32) Brooks, B. R.; Brooks, C. L., 3rd; Mackerell, A. D., Jr.; Nilsson, L.; Petrella, R. J.; Roux, B.; Won, Y.; Archontis, G.; Bartels, C.; Boresch, S.; Caflisch, A.; Caves, L.; Cui, Q.; Dinner, A. R.; Feig, M.; Fischer, S.; Gao, J.; Hodoscek, M.; Im, W.; Kuczera, K.; Lazaridis, T.; Ma, J.; Ovchinnikov, V.; Paci, E.; Pastor, R. W.; Post, C. B.; Pu, J. Z.; Schaefer, M.; Tidor, B.; Venable, R. M.; Woodcock, H. L.; Wu, X.; Yang, W.; York, D. M.; Karplus, M. CHARMM: the biomolecular simulation program. *J. Comput. Chem.* **2009**, *30*, 1545−1614.
(33) Lomize, M. A.; Lomize, A. L.; Pogozheva, I. D.; Mosberg, H. I. OPM: orientations of proteins in membranes database. *Bioinformatics* **2006**, *22*, 623−625.
(34) Cherezov, V.; Rosenbaum, D. M.; Hanson, M. A.; Rasmussen, S. G.; Thian, F. S.; Kobilka, T. S.; Choi, H. J.; Kuhn, P.; Weis, W. I.; Kobilka, B. K.; Stevens, R. C. High-resolution crystal structure of an engineered human β_2-adrenergic G protein-coupled receptor. *Science* **2007**, *318*, 1258−1265.
(35) Kobilka, B. K.; Kobilka, T. S.; Daniel, K.; Regan, J. W.; Caron, M. G.; Lefkowitz, R. J. Chimeric α_2-, β_2-adrenergic receptors: delineation of domains involved in effector coupling and ligand binding specificity. *Science* **1988**, *240*, 1310−1316.
(36) Dror, R. O.; Arlow, D. H.; Borhani, D. W.; Jensen, M. O.; Piana, S.; Shaw, D. E. Identification of two distinct inactive conformations of the β_2-adrenergic receptor reconciles structural and biochemical observations. *Proc. Natl. Acad. Sci. U.S.A.* **2009**, *106*, 4689−4694.
(37) *Maestro v9.3*; Schrödinger, LLC: Portland, OR.
(38) Forli, S. *Raccoon|Autodock VS: An automated tool for preparing AutoDock virtual screenings*. http://autodock.scripps.edu/resources/raccoon (accessed 10/17/2011).
(39) Trott, O.; Olson, A. J. AutoDock Vina: improving the speed and accuracy of docking with a new scoring function, efficient optimization, and multithreading. *J. Comput. Chem.* **2010**, *31*, 455−461.
(40) Jo, S.; Kim, T.; Im, W. Automated builder and database of protein/membrane complexes for molecular dynamics simulations. *PLoS One* **2007**, *2*, e880.
(41) Jo, S.; Lim, J. B.; Klauda, J. B.; Im, W. CHARMM-GUI Membrane Builder for mixed bilayers and its application to yeast membranes. *Biophys. J.* **2009**, *97*, 50−58.

DOI: 10.1021/ct5008907
J. Chem. Theory Comput. 2015, 11, 1255−1266

(42) Jo, S.; Kim, T.; Iyer, V. G.; Im, W. CHARMM-GUI: a web-based graphical user interface for CHARMM. *J. Comput. Chem.* **2008**, *29*, 1859−1865.
(43) Steinbach, P. J.; Brooks, B. R. New spherical-cutoff methods for long-range forces in macromolecular simulation. *J. Comput. Chem.* **1994**, *15*, 667−683.
(44) Essmann, U.; Perera, L.; Berkowitz, M. L.; Darden, T.; Lee, H.; Pedersen, L. G. A smooth particle mesh Ewald method. *J. Chem. Phys.* **1995**, *103*, 8577−8593.
(45) Ryckaert, J. P.; Ciccotti, G.; Berendsen, H. J. C. Numerical-integration of cartesian equations of motion of a system with constraints - molecular-dynamics of N-alkanes. *J. Comput. Phys.* **1977**, *23*, 327−341.
(46) Feller, S. E.; Zhang, Y. H.; Pastor, R. W. Computer-simulation of liquid/liquid interfaces. 2. Surface-tension area dependence of a bilayer and monolayer. *J. Chem. Phys.* **1995**, *103*, 10267−10276.
(47) Jo, S.; Jiang, W.; Lee, H. S.; Roux, B.; Im, W. CHARMM-GUI Ligand Binder for absolute binding free energy calculations and its application. *J. Chem. Inf. Model.* **2013**, *53*, 267−277.
(48) Beglov, D.; Roux, B. Finite representation of an infinite bulk system - solvent boundary potential for computer-simulations. *J. Chem. Phys.* **1994**, *100*, 9050−9063.
(49) Im, W.; Berneche, S.; Roux, B. Generalized solvent boundary potential for computer simulations. *J. Chem. Phys.* **2001**, *114*, 2924−2937.
(50) Deng, Y. Q.; Roux, B. Calculation of standard binding free energies: Aromatic molecules in the T4 lysozyme L99A mutant. *J. Chem. Theory Comput.* **2006**, *2*, 1255−1273.
(51) Wang, J.; Deng, Y.; Roux, B. Absolute binding free energy calculations using molecular dynamics simulations with restraining potentials. *Biophys. J.* **2006**, *91*, 2798−2814.
(52) Ge, X.; Roux, B. Absolute binding free energy calculations of sparsomycin analogs to the bacterial ribosome. *J. Phys. Chem. B* **2010**, *114*, 9525−9539.
(53) Lee, H. S.; Jo, S.; Lim, H. S.; Im, W. Application of binding free energy calculations to prediction of binding modes and affinities of MDM2 and MDMX inhibitors. *J. Chem. Inf. Model.* **2012**, *52*, 1821−1832.
(54) Lin, Y.-L.; Aleksandrov, A.; Simonson, T.; Roux, B. An overview of electrostatic free energy computations for solutions and proteins. *J. Chem. Theory Comput.* **2014**, *10*, 2690−2709.
(55) Aksimentiev, A.; Schulten, K. Imaging α-hemolysin with molecular dynamics: ionic conductance, osmotic permeability, and the electrostatic potential map. *Biophys. J.* **2005**, *88*, 3745−3761.
(56) Humphrey, W.; Dalke, A.; Schulten, K. VMD: visual molecular dynamics. *J. Mol. Graph.* **1996**, *14* (33−38), 27−38.
(57) Baker, J. G. The selectivity of β-adrenoceptor antagonists at the human β_1, β_2 and β_3 adrenoceptors. *Br. J. Pharmacol.* **2005**, *144*, 317−322.
(58) Sabio, M.; Jones, K.; Topiol, S. Use of the X-ray structure of the β_2-adrenergic receptor for drug discovery. Part 2: Identification of active compounds. *Bioorg. Med. Chem. Lett.* **2008**, *18*, 5391−5395.
(59) Vilardaga, J. P.; Bunemann, M.; Krasel, C.; Castro, M.; Lohse, M. J. Measurement of the millisecond activation switch of G protein-coupled receptors in living cells. *Nat. Biotechnol.* **2003**, *21*, 807−812.
(60) Zheng, L.; Chen, M.; Yang, W. Random walk in orthogonal space to achieve efficient free-energy simulation of complex systems. *Proc. Natl. Acad. Sci. U.S.A.* **2008**, *105*, 20227−20232.
(61) Jiang, W.; Roux, B. Free energy perturbation Hamiltonian replica-exchange molecular dynamics (FEP/H-REMD) for Absolute Ligand Binding Free Energy Calculations. *J. Chem. Theory. Comput.* **2010**, *6*, 2559−2565.
(62) Kent, R. S.; De Lean, A.; Lefkowitz, R. J. A quantitative analysis of β-adrenergic receptor interactions: resolution of high and low affinity states of the receptor by computer modeling of ligand binding data. *Mol. Pharmacol.* **1980**, *17*, 14−23.
(63) Zhang, Y.; Skolnick, J. TM-align: a protein structure alignment algorithm based on the TM-score. *Nucleic Acids Res.* **2005**, *33*, 2302−2309.

DOI: 10.1021/ct5008907
J. Chem. Theory Comput. 2015, 11, 1255−1266